Stratigraphic mapping of paintings by multispectral reflectography

Alice Dal Fovo[a] 📧, **Raffaella Fontana**

National Research Council - National Institute of Optics (CNR-INO), Largo E. Fermi 6, 50125 Florence, Italy

Abstract Despite recent technological advances, it is currently not possible to uniquely and noninvasively measure the micrometric thickness of pictorial layers in paintings. The presence of optically opaque materials (pigments) severely limits the detection capability, as it hinders the penetration of the probe's near-infrared radiation, typically employed for this purpose. In our previous work, we explored the possibility of using diffuse reflectance spectroscopy (DRS) to achieve stratigraphic information about painting materials. We showed that the thickness of pictorial layers can be quantified by the intensity of the spectral reflectance factor measured at a given wavelength in the infrared, i.e., an easily detectable spectral feature. In the present work, we extend the previously proposed method by applying multispectral reflectography to measure new ad hoc prepared pictorial samples and a mock-up simulating a Mondrian painting. We thus demonstrate that it is possible to obtain 2D and 3D stratigraphic maps of the pictorial layer over large areas with the same measurement time and spatial resolution as multispectral scanning reflectography.

1 Introduction

Technologies used for artwork diagnostics are constantly advancing to define increasingly versatile and effective analysis protocols and to adapt methodologies to the huge variety of materials and art objects. The analysis of the multilayer structure that characterizes paintings is of great importance not only for an assessment of the state of conservation but also to support and monitor an informed restoration intervention. To date, the micrometric thickness of pictorial layers is often impossible to measure except through microscopic cross-sectional observation of sampled fragments. The invasive approach, however, is often avoided in the field of heritage science (HS), as it is generally preferred not to remove the original material in order to preserve the integrity of the artwork. In addition, when sampling is allowed, it is done in the marginal areas of the painting or on the edges of lacunae. The stratigraphic measurements thus obtained are not always representative of the entire pictorial layer, which in fact can vary greatly in thickness. The non-invasive approach, on the other hand, relies on optical technologies using low-intensity radiation probes, the penetration of which is often hindered by the presence of optically opaque materials. Most pigments dispersed in the painting medium exhibit absorption or scattering properties that limit the in-depth survey to a few microns. Among the most widely used noninvasive techniques, optical coherent tomography (OCT) [1] allows for the cross-sectional examination of layers that are semi-transparent to infrared radiation [2, 3]. Therefore, OCT is particularly suitable for the analysis of coating materials such as varnishes, but stratigraphic measurements of pictorial layers with OCT are often very limited for the aforementioned [4]. Alternative techniques recently introduced in HS from the biological and medical field are nonlinear optical microscopies (NLOM) [5, 6], namely second and third harmonic generation (SHG and THG) [7] and multiphoton excitation fluorescence (MPEF) [8]. These modalities have shown great potential for the analysis of a wide range of art materials. By using femtosecond pulsed lasers tightly focused by high numerical aperture objective, it is possible to exploit the nonlinear susceptibility of materials with a penetration and axial resolution capability superior to linear optical techniques, while using non-damaging NIR radiation. In addition, SH, TH and MPEF signals can be generated and collected simultaneously to achieve chemical, stratigraphic and morphological information, in a single measurement. However, even NLOM techniques show limited depth detectability of pictorial layers due to the optical opacity of many pigments [9]. In recent years, photoacoustics (PA) [10] was proposed for stratigraphic measurements in painting as it exploits the presence of absorbing materials in the NIR to generate acoustic waves. Based on the principle of exponential frequency attenuation and knowing the attenuation coefficient of the medium, it is possible to quantify the thickness of a material by analysing the frequency of the transmitted acoustic waves [11]. This method has been tested on pictorial mock-ups [12] and on a historical painting [13], demonstrating high potential in the cultural heritage field. The main limitation of PA is the need to use a coupling medium to enhance the transmission of the acoustic waves from the material to the transducer. Although nonaggressive coupling media have been used on the surface of paintings, such as carboxymethylcellulose and agar gels [14, 15], this measurement involves a contact that does not fully comply with the principle of non-invasiveness. Recent studies have shown that it is possible to bypass the application of a medium by using air-coupled

---

[a] e-mail: alice.dalfovo@ino.cnr.it (corresponding author)

transducers with higher sensitivity [16]. However, this method has not yet been tested for stratigraphic measurements. In addition, the most effective measurement configuration for thickness analysis is in transmission mode, which hampers the application of the technique (e.g. on panel paintings). Finally, to date, PA stratigraphic analysis in imaging mode requires rather long measurement times.

In our previous work [17], we explored the possibility of using diffuse reflectance spectroscopy (DRS) to obtain stratigraphic information on paintings. We showed that the thickness of paint layers can be quantified based on the reflectance value measured at a given wavelength in the infrared, i.e., at a characteristic and easily detectable spectral feature. Ten acrylic paints were laid in layers of increasing thickness, which was measured by OCT and correlated with reflectance values measured with fibre optics reflectance spectroscopy (FORS) and reflectance imaging spectroscopy (RIS). We defined an optimized FORS procedure to both stabilize the signal intensity at each measurement and minimize fluctuations, performing consecutive acquisitions interleaved with dark correction by automatic closure of the device shutter to check the signal stability. Nonlinear fitting curves were calculated for each paint, which were used for point-measurement of a paint layer of unknown thickness.

In this work, we have extended the previously proposed approach by applying multispectral reflectography to new ad hoc prepared painting samples and a mock-up simulating a painting by Mondrian. The goal was to obtain stratigraphic 2D and 3D information on the paint layer over large areas with the same measurement time and spatial resolution as multispectral scanning reflectography.

2 Materials and methods

2.1 Painting mock-ups

We prepared the paint samples (Fig. 1a) using three acrylic paints (extra-fine acrylic colours—Maimeri Brera™, Milan, Italy), namely Lemon Yellow (LY), Primary Red Magenta (PRM) and Cobalt Blue (CB). For each paint, the chemical composition and the commercial code are reported in Table 1. On the surface of the wooden support, we laid a layer of acrylic primer (Lefranc Bourgeois™, Paris, France), which was accurately smoothed with fine-grit sandpaper. Afterwards, we drew three vertical lines with a graphite pencil to create an underlying graphic trait, which was then covered by the paint. Finally, we laid each acrylic colour on five adjacent areas of ~ 1 cm^2 (1–5 in Fig. 1a) with increasing thicknesses. To this aim, we overlaid 1 to 5 layers of a nearly 50 µm thick tape (Kapton Cypress—DuPont™, Wilmington, DE, USA) on both sides of the area to be painted to achieve the desired thickness. We spread the paints to obtain increasing thicknesses by using a glass spatula to make their surface as even as possible.

We used the same acrylic paints for the mock-up (Fig. 1b) simulating the painting "Composition in Red, Yellow, Blue and Black" (1921) by Piet Mondrian. The latter was originally designed for hands-on demonstrations of IR reflectography to introduce heritage science and non-invasive technologies to a wider audience, especially young people. The wooden support (size 26×45 cm^2) was prepared in the same way as the acrylic samples described above. The sanded surface of the acrylic primer was divided into squares separated by black lines (black acrylic paint). In three squares, preparatory drawings depicting cartoon characters were made with graphite. Then, the areas with drawings were covered with PRM, LY and CB in imitation of the original painting.

Fig. 1 a RGB image of LY, PRM and CB paint layers with increasing thickness (1 to 5); **b** RGB image of the painting mock-up
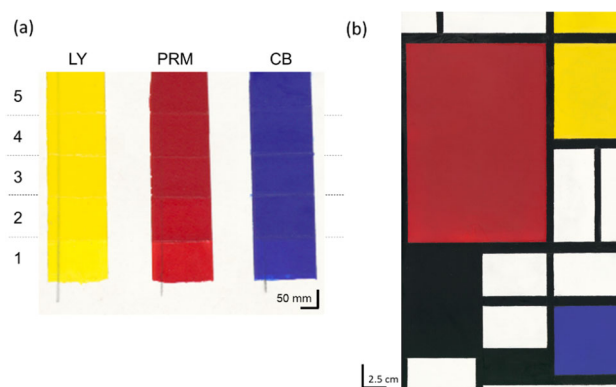
Table 1 The analysed acrylic paints with their chemical composition (as declared by the manufacturer) and commercial code

Paint with Acronym	Chemical composition and commercial code (Maimeri Brera™)
Lemon Yellow (LY)	Benzimidazolone [$C_7H_4N_2O$], PY175—11,784
Primary Red Magenta (PRM)	Quinacridone [$C_{20}H_{12}N_2O_2$], PV19—73,900
Cobalt Blue (CB)	Cobalt(II) Aluminate [$CoAl_2O_4$], PB28—77,346

Fig. 2 Workflow of the method
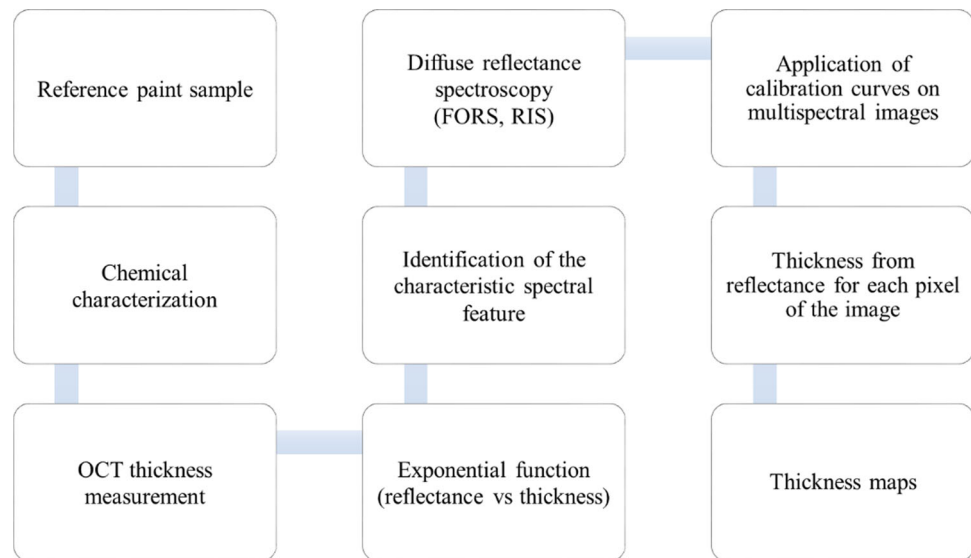
2.2 Spectral-domain optical coherence tomography (Sd-OCT)

The OCT device used in this study is a Thorlabs Telesto-II, working in the 1300 nm regime, with an axial resolution of 5.5 μm in air and a lateral resolution of 13 μm. The maximum field of view (FOV) is 10×10 mm^2, with a 3.5 mm imaging depth. The system is controlled via a 64-bit software running on a high-performance computer. The 3D scanning probe with an integrated video camera allows for high-speed imaging (76 kHz) for rapid volume acquisition and live display. The sample stage provides XY translation and rotation of the sample along with the axial travel of the probe. The 2D tomograms were acquired with a pixel size of 3.5 μm^2.

2.3 Reflectance Imaging Spectroscopy (RIS)

The multispectral scanner developed at CNR-INO is extensively described in [18]. It operates in the range 395–2550 nm and provides simultaneously 32 narrow-band images (16 VIS + 16 NIR) and pointwise spectral information. The joint movement of the lighting system and the collecting optics, placed in a 45°/0° illumination/detection geometry, allows for uniform illumination and minimal heating of the surface. The scanning is carried out with 250 μm sampling step (4 points/mm) and 500 mm/s maximum speed, while an autofocus system ensures the optimal target-lens distance. Before each measurement, a proper adjustment procedure is performed by measuring a suitable standard with a known reflectance value (100% reflectance reference standard, Spectralon™) and background noise, following CIE indications for non-contact spectrophotometric measurements. Both the NIR images and the spectra reported in this work are extracted from the spectral cube using an in-house developed software. To obtain the calibration curves from the reference samples, the average spectrum over a $\varnothing = 8$ mm region (~ 800 pixels on the RIS image), the same measured with OCT, was extracted for each of the five areas. The final thickness maps were computed from the reflectance images taking into account the spectral values pixel by pixel of the entire painted surface.

2.4 Methodology for thickness measurement with RIS

The proposed method, illustrated in the workflow diagram in Fig. 2, consists of a succession of steps beginning with the preparation of ad hoc reference samples, i.e., paint layers of known chemical composition and increasing thickness. The reflectance behaviour of the paint and the thickness of the layers are characterized by reflectance spectroscopy (FORS, RIS) and OCT, respectively. Based on the significant spectral features, identified with the first and second derivatives of the reflectance spectra, exponential functions of reflectance versus thickness are obtained for each paint, which are used as calibration curves for thickness measurements. The process culminates with thickness mapping over large areas of the sample by multispectral reflectography: based on the previously calculated calibration curve, a thickness value is assigned to each pixel in the NIR image at the selected wavelength. The method is validated by comparing the multispectral thickness maps with the OCT measurement previously performed on the reference sample. Finally, the calibration curve is used to calculate thickness maps on an unknown thickness painting, following the same procedure.

Fig. 3 OCT stratigraphic images of LY, PRM and CB, showing the increasing thickness of the paint layers (1–5) laid on the preparation background. The thickness was calculated as the geometrical distance between the air–paint and the paint–background interfaces, with the latter highlighted by the cyan line
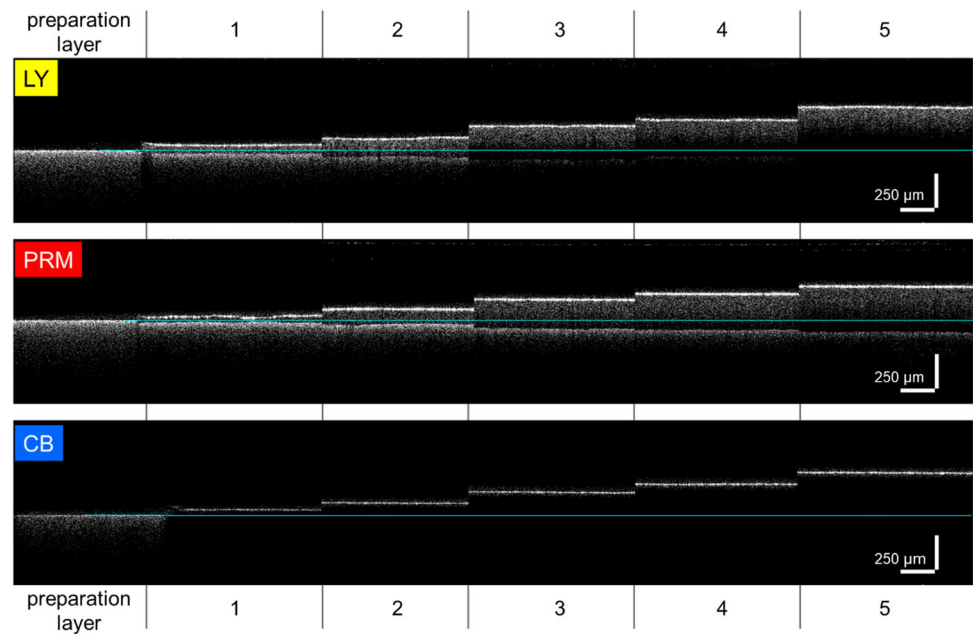
3 Results

Four XZ tomograms (7×1.2 mm^2, pixel size 3.5 μm^2) were acquired on each painted area with spectral-domain optical coherence tomography (Sd-OCT). Given the low transparency of most of the analysed paints, the layer thickness was measured by taking the signal generated at the interface air-background (visible at the edges of each painted area) as a reference, as shown in Fig. 3. The thickness of each pictorial layer was calculated as the average over 20 values, resulting in a range between 30 (area 1) and 300 μm (area 5) for the three acrylics. For each thickness, the error, i.e., the standard deviation, resulted below 6 μm for all areas, demonstrating the micrometric homogeneity of the paint layers.

Multispectral reflectography was performed on all samples to extract the spectral data allowing for the identification of the characteristic spectral feature for each acrylic paint. For each area (1–5), the average spectra are plotted together with the spectrum of the underlying preparation layer in Fig. 4a, b, c for LY, PRM and CB, respectively. The first and second derivatives (not reported) were computed for all spectra to facilitate the identification of the spectral feature best representing the reflectance dependence on the material thickness. Based on our previous study [17], we selected the maximum point at 765 nm and 850 nm for PRM and CB, respectively. For LY, analysed here for the first time, the inflection point at 1400 nm was identified as the characteristic feature suitable for our aim. The reflectance values of the identified spectral feature are plotted as a function of the corresponding OCT thickness in Fig. 4d, e, f. As observed in our previous work [17], the reflectance decreases exponentially with increasing paint thickness, for all acrylics. Therefore, the trend of the reflectance as a function of the thickness is expressed by the following equation (in accordance with Lambert–Beer law for the absorption):

$$y = y_0 + Ae^{R_0 z} \tag{1}$$

where y = R%, y_0 = offset, A = initial value, R_0 = growth constant, and z = layer thickness. The fit parameters for the three paints are reported in Table 2, together with the adjusted R-square parameter (R^2) expressing the quality of the fit.

For each acrylic paint, 2D and 3D thickness images were processed in MATLAB environment using the above-described fit curves and applying the procedure illustrated in Fig. 2. First, we examined the samples layers with increasing thickness: NIR images at 1400 nm, 765 nm and 850 nm were used to obtain the thicknesses of LY, PRM and CB, respectively (Fig. 5a, c, e). The thickness value of each pixel in the image was then derived from the corresponding reflectance value, according to Eq. 1. The resulting thickness 2D maps are reported as colour-coded images in Fig. 5b, d, f.

The presence of the graphite trait underneath the paint layers is clearly visible in the NIR images, due to the absorbing properties of this material in the near-infrared spectral range. Therefore, in correspondence of the graphite line, the reflectance values are extremely low. Following the exponential behaviour of Fig. 4 d, e, f, the high absorbance (small reflectance) results in high thickness values (reddish appearance in the colour map) that are not real and therefore should not be considered when measuring the thickness of the pictorial layer. Consequently, the 3D mesh shown in Fig. 6b was calculated on the acrylic PRM area by omitting the graphite line (Fig. 6a).

To evaluate the method's precision, thickness values obtained with RIS were compared with the reference thicknesses measured with OCT. For this purpose, areas of 29×31 pixel (corresponding to 7.25×7.75 mm) were selected on the colour-coded thickness
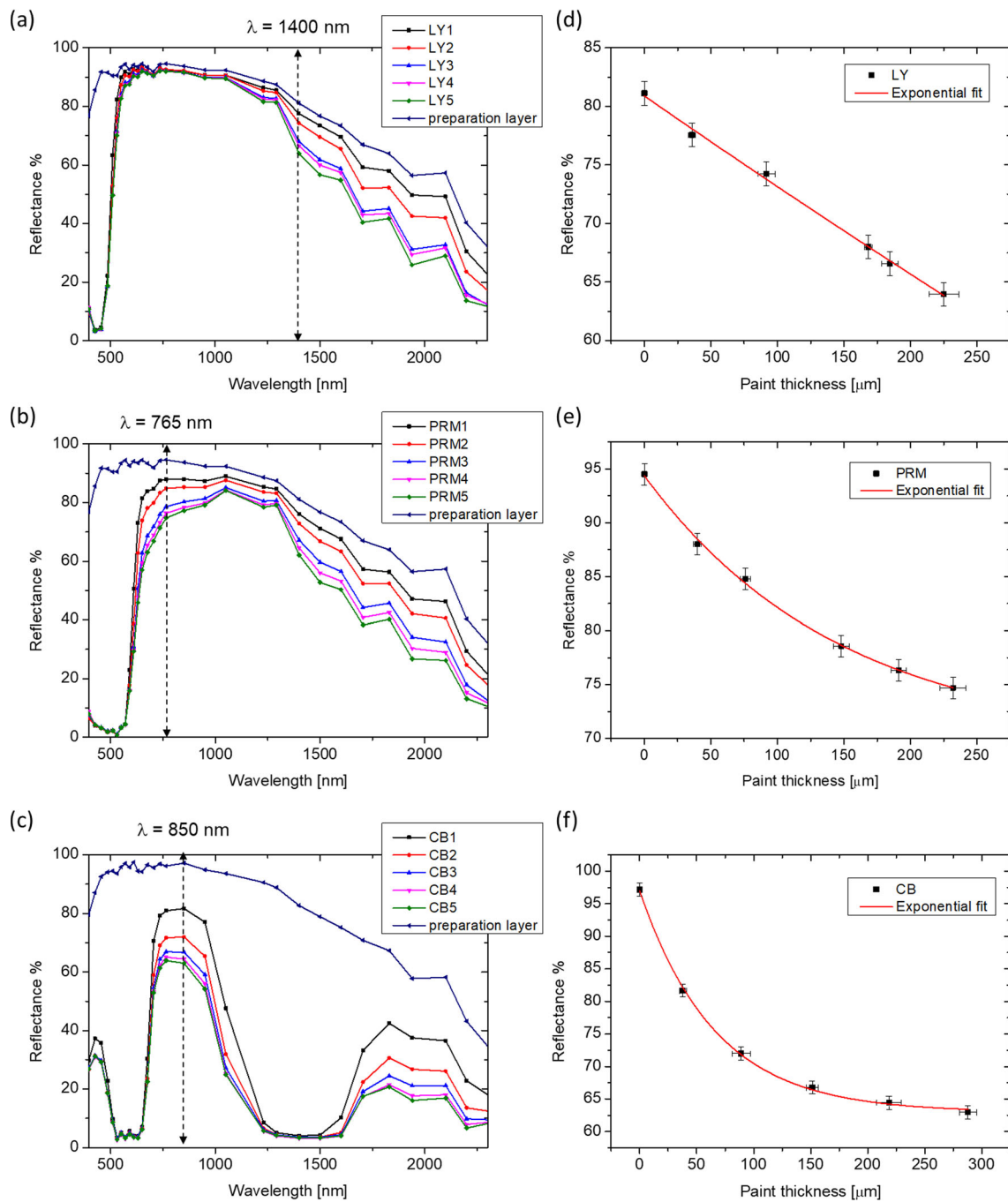
Fig. 4 Reflectance spectra acquired on LY (a), PRM (b) and CB (c) paint samples for each layer thickness (1–5) reported with the spectrum of the preparation background; the dashed arrow points out the spectral wavelength at which the reflectance R% values were measured and then plotted as a function of the five OCT thicknesses (d, e, f). The preparation layer is assumed to be of zero thickness. The length of the error bars is the standard deviation of each dataset. Red lines represent the fitting exponential functions

maps on each layer, avoiding the underlying graphite line, as shown in Fig. 7 for the LY sample, as an example. The magnification of each area (Fig. 7 b-f) allows for the visualization of the colour-coded thickness for each image pixel. The mean thicknesses were calculated with their standard deviation for each selected area. Results are shown in comparison with the corresponding OCT values in Table 3. The differences between the values calculated by the two methods are, in all cases, within the experimental errors, except for area 2 of LY (less than 1 μm). The standard deviation is generally higher for values calculated from RIS maps than for OCT values. These differences, although not substantial, can be attributed to the fact that the thickness measurement by OCT was carried out on XZ sections that also include the edges of the pictorial layer, whereas the areas selected on the RIS maps are located in the centre of each layer.

Table 2 For each paint, we report the fit parameters of the exponential function (1) describing the dependence of the reflectance of the spectral feature identified with multispectral scanning on the layer thickness

Paint	Spectral feature, λ [nm]	Fitting parameters			R^2
		$y0$	A	$R0$	
LY	flex, 1400	−135.02	215.9	-3.65×10^{-4}	0.995
PRM	max, 765	69.58	24.78	-6.79×10^{-3}	0.997
CB	max, 850	62.98	34.03	-1.52×10^{-2}	0.998
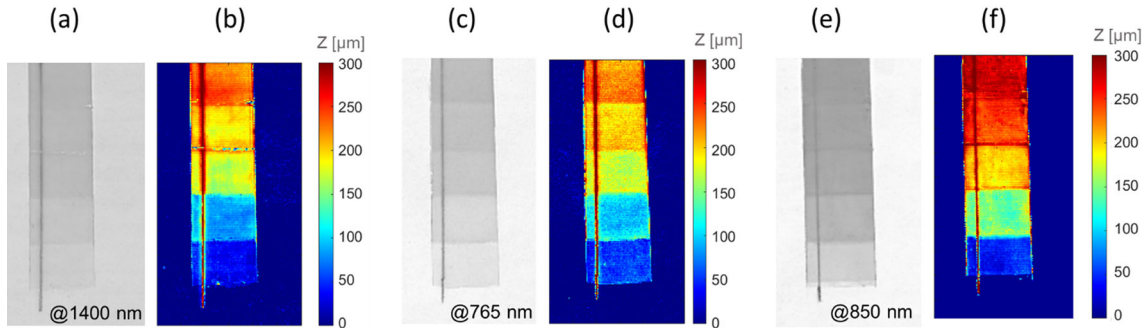
Fig. 5 NIR images and colour-coded thickness images of samples LY (**a**, **b**), PRM (**c**, **d**) and CB (**e**, **f**)
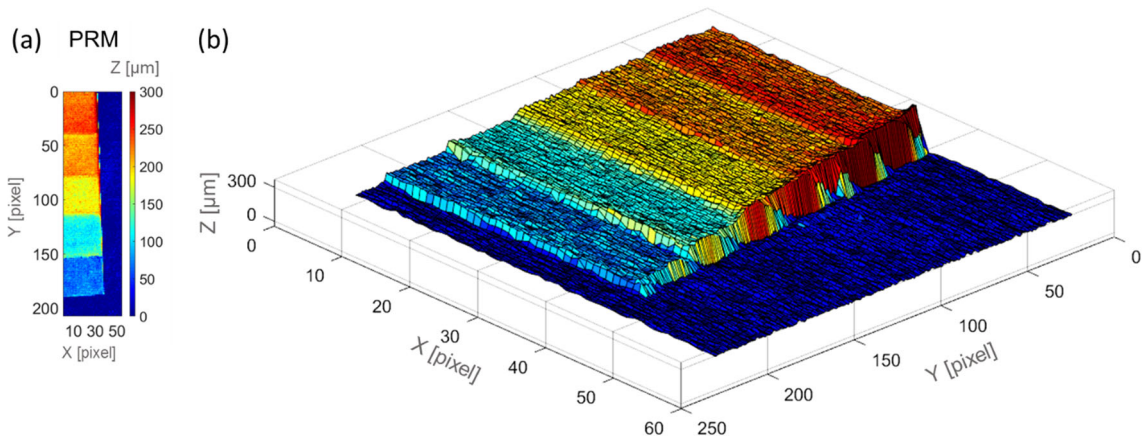
Fig. 6 Colour-coded thickness image of PRM sample excluding the graphite line (**a**) and corresponding 3D stratigraphic map (**b**). The pixel size on X and Y axes is 250 µm

Table 3 Mean thickness calculated with RIS and OCT for each selected area on samples LY, PRM and CB. For each thickness value, the respective standard deviation is reported in brackets

Area	LY		PRM		CB	
	Mean thickness (St. Dev.) [µm]		Mean thickness (St. Dev.) [µm]		Mean thickness (St. Dev.) [µm]	
	OCT	RIS	OCT	RIS	OCT	RIS
5	225.01 (11.28)	227.08 (11.20)	231.86 (9.76)	239.70 (13.30)	287.77 (7.50)	290. 62 (10.36)
4	184.6 (6.15)	188.33 (8.47)	191.03 (5.68)	197.07 (11.31)	218.76 (10.84)	212.50 (10.36)
3	168.21 (2.73)	167.19 (9.19)	147.99 (6.04)	164.51 (11.37)	151.32 (5.16)	163.28 (10.85)
2	91.75 (6.46)	79.09 (6.81)	75.88 (3.86)	83.05 (11.87)	88.97 (8.04)	88.38 (15.50)
1	35.77 (2.70)	33.19 (8.11)	39.71 (2.66)	47.37 (10.44)	37.94 (3.10)	42.65 (14.14)

Finally, the same approach was tested on the painting mock-up. In Fig. 8a and b the details of the NIR images at 1400 nm, 765 nm and 850 nm and the 2D thickness maps are superimposed on the LY, PRM and CB areas in the RGB image, respectively, allowing for both visualization of the underdrawing and micrometric measurement of the paint thickness. Based on the colour scale, the thickness of LY, PRM and CB results in the range 60–150 µm, 70–240 µm and 60–190 µm, respectively.

The NIR image and 3D colour map of a detail of the PRM area are shown in Fig. 9, where three labels display the position (X, Y) in pixel and the thickness of the paint layer (Z) in micron in three selected points (1, 2, 3).
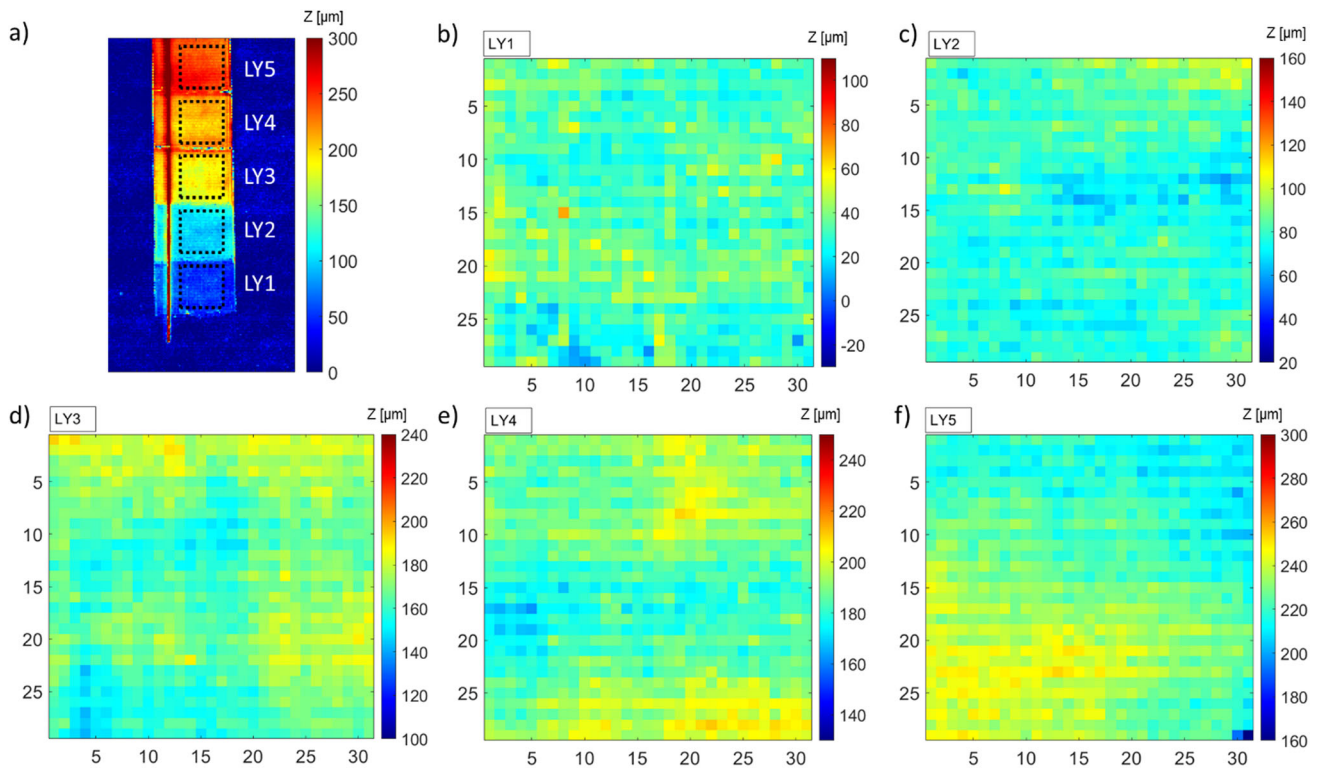
Fig. 7 Thickness measurement with multispectral reflectography on LY sample: colour-coded map and dashed rectangle defining the areas (size: 7.25 × 7.75 mm) selected for average thickness calculation (**a**); magnification of the five areas (**b–f**) highlighting the thickness value for each pixel

Fig. 8 a RGB image of the painting mock-up; **b** details of NIR images of LY (at 1400 nm), PRM (at 756 nm) and CB (at 850 nm) superimposed on the RGB image of the painting; **c** corresponding colour-scaled stratigraphic images allowing for both the visualization of the underdrawing and micrometric measurement of the paint thickness. As explained above, the apparent thickness of the drawing is due to the absorbance properties of graphite and, thus, should not be considered for the measurement of the paint layer
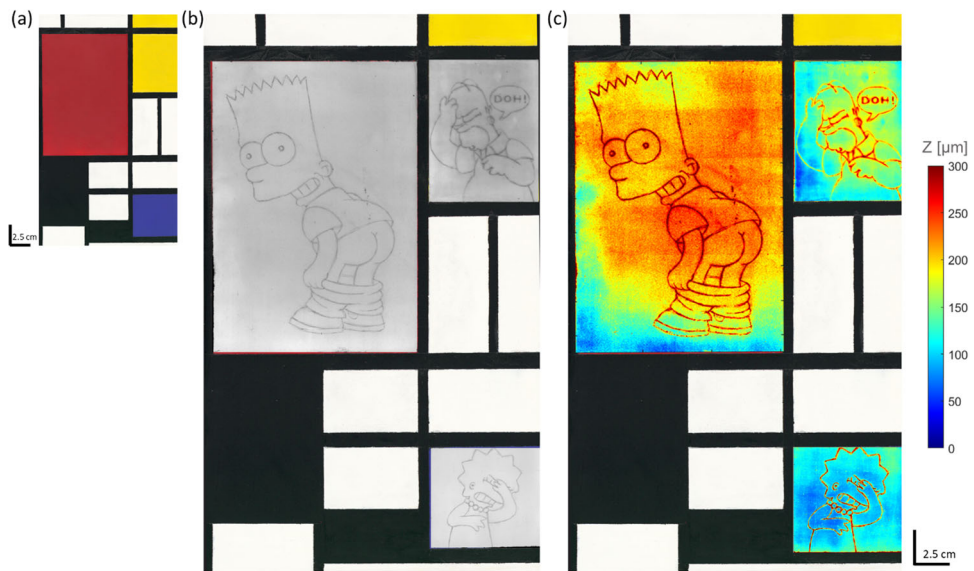
The thickness of PRM paint was measured at points 1, 2 and 3 by OCT for comparison (see Fig. 1 in the Supplementary Material). The optical distance between the air/paint and paint/preparation interfaces was corrected for the refractive index (n = 1.37) calculated for PRM in our previous work [17]. The true thickness resulted $144 \pm 3.5\ \mu m$, $198 \pm 3.5\ \mu m$ and $224 \pm 3.5\ \mu m$ for points 1, 2 and 3, respectively, in good agreement with the thickness values obtained from RIS images with the proposed method.
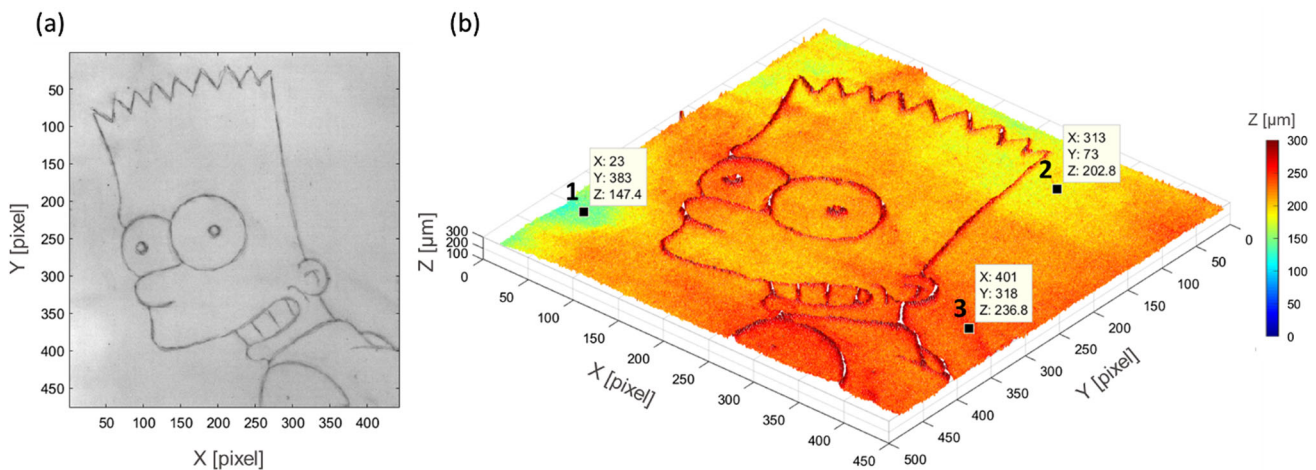
Fig. 9 Detail of the PRM rectangle: **a** NIR image at 765 nm showing the underdrawing; **b** 3D stratigraphic map: the labels report the position (X, Y) in pixel of three selected points (1, 2, 3) and the thickness of the paint layer (Z) in micron

4 Discussion

The feasibility of the proposed method was demonstrated on single layers of homogeneous paints. For more complex cases, such as layers stratifications, pigments mixtures, different binders and coloured preparation layer, which are commonly found in painted artworks, more heterogeneous samples should be prepared and measured in order to build an increasingly representative database of calibration curves. Advanced technologies can be used for automated spectral feature extraction and calibration curve calculation. Machine learning is widely employed in the biomedical field [19, 20] and it has been recently introduced in CH studies [21, 22] to extract optical properties from diffuse reflectance data. However, we exclude that the thickness of highly opaque paints, which exhibit a constant R% value in the examined spectral range regardless of layer thickness, can be determined by this method. For paints showing transparency in the considered spectral range, instead, the selection of the characteristic spectral feature is made on the basis of its significance: it can either be characteristic of a given paint or allow for the recognition of an appreciable difference in the measured reflectance values with increasing material thickness. If these criteria are met, the resulting thickness maps are in perfect agreement, regardless of the spectral feature (wavelength) selected for analysis. Indeed, since the thickness of the reference samples are known and constant, for each selected spectral feature a calibration curve can be obtained and used to determine the unknown thickness of the same paint. This issue is clearly demonstrated by the results of the analysis at different wavelengths (1400 nm, 1500 nm and 1600 nm) of LY paint, for both the sample and the mock-up, shown as an example in Fig. 2 in the Supplementary Material. Fit parameters of the exponential function describing the dependence of the reflectance at the different wavelengths on the layer thickness are reported in Table 1 SM.

The suitability of multispectral reflectography for thickness mapping was assessed by comparison with the reference method for stratigraphic measurements, OCT. Due to the low transparency of the paints to OCT radiation, the real thickness of the paint layers was calculated with respect to the substrate, i.e., the portion of the visible preparation not covered by the paint layer. In paintings, where the preparation layer cannot be taken as a reference, it is necessary to know a priori the refractive index of the material to correct the optical distances in OCT tomograms. However, the refractive index of the paints analysed at the OCT wavelength, typically in the IR, is not known (average values and data are found in the literature only in the visible, and not even for all pigments), and therefore, the actual thickness can never be univocally determined. Therefore, measuring the thickness of a pictorial layer from its spectral characteristics can overcome some limitations of OCT technique.

5 Conclusions

In this work, we analysed the thicknesses of a set of single-layer painted samples with underdrawing, which was measured with OCT and correlated to the reflectance value measured by DRS to obtain calibration curves. The results demonstrate that it is possible to obtain 2D and 3D thickness maps of pictorial layers through multispectral reflectography, exploiting the transparency of pigments in narrow spectral ranges where it is possible to identify significant spectral features. The main advantage of this approach is the capability to analyse large areas in a fully non-invasive way with the acquisition times of scanning reflectography. This is not possible through the technologies used to date for this purpose. Furthermore, the acrylic paints used in this work are characterized by an optical opacity which does not allow their thickness to be measured using OCT, except by taking the visible preparation support as a reference (as was done in this case). This demonstrates that the proposed method overcomes the main detectability limits of

other stratigraphic non-invasive techniques. An additional advantage is the ability to visualize possible underdrawings directly in the thickness map.

Future developments of this approach include expanding the calibration curves database to include tempera paints with different paint media, as well as applying the method to multilayered paint samples.

Declarations

Conflict of interest The authors declares that they have no conflicts of interest.

References

1. P. Targowski, M. Kowalska, M. Sylwestrzak, M. Iwanicka, OCT for examination of cultural heritage objects. In *Optical Coherence Tomography and Its Non-medical Applications*. IntechOpen, (2020) p. 147–164 (doi: dx.doi.org/https://doi.org/10.5772/intechopen.88215).
2. T. Callewaert, J. Guo, G. Harteveld, A. Vandivere, E. Eisemann, J. Dik, J. Kalkman, Multi-scale optical coherence tomography imaging and visualization of Vermeer's girl with a pearl earring. Opt. Exp. **28**(18), 26239–26256 (2020)
3. H. Liang, M.G. Cid, R.G. Cucu, G.M. Dobre, A.G. Podoleanu, J. Pedro, D. Saunders, En-face optical coher-ence tomography-a novel application of non-invasive imaging to art conservation. Opt. Exp. **13**(16), 6133–6144 (2005)
4. P. Targowski, M. Iwanicka, Optical coherence tomography: its role in the non-invasive structural examination and conservation of cultural heritage objects—a review. Appl. Phys. A **106**, 265–277 (2012)
5. A. Dal Fovo, M. Castillejo, R. Fontana, Nonlinear optical microscopy for artworks physics. La Riv. Del Nuovo Cim. **44**, 453–498 (2021)
6. M. Mari, G. Filippidis, Non-linear microscopy: a well-established technique for biological applications towards serving as a diagnostic tool for in situ cultural heritage studies. Sustainability **12**(4), 1409 (2020)
7. D. Oron, D. Yelin, E. Tal, S. Raz, R. Fachima, Y. Silberberg, Depth-resolved structural imaging by third-harmonic generation microscopy. J. Struct. Biol. **147**(1), 3–11 (2004)
8. E. Gratton, N.P. Barry, S. Beretta, A. Celli, Multiphoton fluorescence microscopy. Methods **25**(1), 103–110 (2001)
9. A. Dal Fovo, M. Sanz, M. Oujja, R. Fontana, S. Mattana, R. Cicchi, P. Targowski, M. Sylwestrzak, A. Romani, C. Grazia et al., In-depth analysis of egg-tempera paint layers by multiphoton excitation fluorescence microscopy. Sustainability **12**, 3831 (2020)
10. G.J. Tserevelakis, I. Vrouvaki, P. Siozos, K. Melessanaki, K. Hatzigiannakis, C. Fotakis, G. Zacharakis, Photoacoustic imaging reveals hidden under-drawings in paintings. Sci. Rep. **7**(1), 747 (2017)
11. G.J. Tserevelakis, A. Dal Fovo, K. Melessanaki, R. Fontana, G. Zacharakis, Photoacoustic signal attenuation analysis for the assessment of thin layers thickness in paintings. J. Appl. Phys., 123(12). (2018)
12. A. Dal Fovo, G.J. Tserevelakis, A. Papanikolaou, G. Zacharakis, R. Fontana, Combined photoacoustic imaging to delineate the internal structure of paintings. Opt. Lett. **44**(4), 919–922 (2019)
13. A. Dal Fovo, G.J. Tserevelakis, E. Klironomou, G. Zacharakis, R. Fontana, First combined application of photoacoustic and optical techniques to the study of an historical oil painting. Eur. Phys. J. Plus **136**(7), 757 (2021)
14. A. Chaban, G.J. Tserevelakis, E. Klironomou, G. Zacharakis, J. Striova, Agar gel as a non-invasive coupling medium for reflectance photoacoustic (PA) imaging: experimental results on wall-painting mock-Ups. J. Imag. **8**(9), 235 (2022)
15. F.A. Pisu, D. Chiriu, E. Klironomou, G. Zacharakis, G.J. Tserevelakis, Stratigraphy of fresco paintings: a new approach with photoacoustic and SORS imaging. J. Imag. **9**(1), 16 (2023)
16. G.J. Tserevelakis, P. Siozos, A. Papanikolaou, K. Melessanaki, G. Zacharakis, Non-invasive photoacoustic detection of hidden underdrawings in paintings using air-coupled transducers. Ultrasonics **98**, 94–98 (2019)
17. A. Dal Fovo, M. Martínez-Weinbaum, M. Oujja, M. Castillejo, R. Fontana, Reflectance spectroscopy as a novel tool for thickness measurements of paint layers. Molecules **28**(12), 4683 (2023)
18. J. Striova, C. Ruberto, M. Barucci, J. Blažek, D. Kunzelman, A. Dal Fovo, R. Fontana, Spectral imaging and archival data in analysing Madonna of the Rabbit paintings by Manet and Titian. Angew. Chem. **130**(25), 7530–7534 (2018)
19. F. Geldof, B. Dashtbozorg, B.H. Hendriks, H.J. Sterenborg, T.J. Ruers, Layer thickness prediction and tissue classification in two-layered tissue structures using diffuse reflectance spectroscopy. Sci. Rep. **12**(1), 1698 (2022)
20. M.H. Nguyen, Y. Zhang, F. Wang, De. La Garza, J. Evia Linan, M.K. Markey, J.W. Tunnell, Machine learning to extract physiological parameters from multispectral diffuse reflectance spectroscopy. J. Biomed. Opt. **26**(5), 052912–052912 (2021)
21. T. Kleynhans, C.M. Schmidt Patterson, K.A. Dooley, D.W. Messinger, J.K. Delaney, An alternative approach to mapping pigments in paintings with hyperspectral reflectance image cubes using artificial intelligence. Heritage Sci. **8**(1), 1–16 (2020)
22. L. Liu, T. Miteva, G. Delnevo, S. Mirri, P. Walter, L. de Viguerie, E. Pouyet, Neural networks for hyperspectral imaging of historical paintings: a practical review. Sensors **23**(5), 2419 (2023)